HHS Public Access

Author manuscript

Nat Med. Author manuscript; available in PMC 2020 January 03.

Published in final edited form as:

Nat Med. 2019 July ; 25(7): 1057–1063. doi:10.1038/s41591-019-0498-z.

Programmable bacteria induce durable tumor regression and systemic antitumor immunity

Sreyan Chowdhury[1,2], **Samuel Castro**[1], **Courtney Coker**[1], **Taylor E. Hinchliffe**[1], **Nicholas Arpaia**[2,3,*], **Tal Danino**[1,3,4,*]

[1]Department of Biomedical Engineering, Columbia University, New York, NY 10027, USA

[2]Department of Microbiology & Immunology, Vagelos College of Physicians and Surgeons of Columbia University, New York, NY 10032, USA

[3]Herbert Irving Comprehensive Cancer Center, Columbia University, New York, NY 10032, USA

[4]Data Science Institute, Columbia University, New York, NY 10027, USA

SUMMARY PARAGRAPH

Synthetic biology is driving a new era of medicine through the genetic programming of living cells[1,2]. This transformative approach allows for the creation of engineered systems that intelligently sense and respond to diverse environments, ultimately adding specificity and efficacy that extends beyond the capabilities of molecular-based therapeutics[3–6]. One particular focus area has been the engineering of bacteria as therapeutic delivery systems to selectively release therapeutic payloads *in vivo*[7–11]. Here, we engineered a non-pathogenic *E. coli* to specifically lyse within the tumor microenvironment and release an encoded nanobody antagonist of CD47 (CD47nb)[12], an anti-phagocytic receptor commonly overexpressed in several human cancers[13,14]. We show that delivery of CD47nb by tumor-colonizing bacteria increases activation of tumor-infiltrating T cells, stimulates rapid tumor regression, prevents metastasis, and leads to long-term survival in a syngeneic tumor model. Moreover, we report that local injection of CD47nb bacteria stimulates systemic tumor antigen–specific immune responses that reduce the growth of untreated tumors – providing, to the best of our knowledge, the first demonstration of an abscopal effect induced by an engineered bacterial immunotherapy. Thus, engineered bacteria may be used for safe and local delivery of immunotherapeutic payloads leading to systemic antitumor immunity.

The origins of cancer immunotherapy trace back to the pioneering work of Dr. William Coley, who observed tumor clearance in some patients that received injections of bacteria[15] – a result now attributed to leukocyte activation[16–18]. Since then, a multitude of studies have

---

*Co-corresponding authors.

AUTHOR CONTRIBUTIONS

S.C., N.A. and T.D. conceived and designed the study. S.C., T.E.H., C.C., and S.C. performed *in vivo* experiments. S.C performed *in vitro* characterization of eSLC-CD47nb and conducted immunophenotyping experiments. S.C., N.A. and T.D. analyzed data and wrote the manuscript with input from all other authors.

COMPETING INTERESTS STATEMENT

S.C., N.A. and T.D. have filed a provisional patent application with the US Patent and Trademark Office (US Patent Application No. 62/747,826) related to this work. T.D. and N.A. have a financial interest in GenCirq, Inc..

demonstrated that bacteria preferentially grow within tumor cores due to the immunoprivileged nature of the often hypoxic and necrotic tumor microenvironment, and can locally affect tumor growth through the recruitment and activation of the immune system[19–23]. With the advent of synthetic biology over the past two decades and the development of numerous bacteria gene circuits[6,24–28], we reasoned that programming bacteria to controllably release recombinant immunotherapies could allow for local delivery of higher effective concentrations of therapy while preventing toxicities observed following systemic delivery of identical or similar therapeutic agents.

To test the efficacy of this approach, we chose to target CD47, a potent anti-phagocytic receptor overexpressed in several human cancers[13,14,29]. Recent studies have shown that CD47 blockade not only increases phagocytosis of cancer cells but also promotes cross presentation of tumor antigens by dendritic cells to enhance priming of antitumor effector T cells in syngeneic murine tumor models[12,30–32]. However, as demonstrated in both preclinical models[33] and human trials[34,35], CD47 blockade using systemically delivered antibodies can result in anemia and thrombocytopenia due to high expression of CD47 on red blood cells and platelets respectively. To improve upon its therapeutic profile, a nanobody (camelid single heavy chain antibody fragment) against CD47 with ~200-fold higher binding affinity than the commercially available anti-mouse CD47 monoclonal antibody (miap301) was recently developed and characterized[12]. This nanobody demonstrated mild effects as a systemically administered monotherapy, potentially due to lack of Fc-mediated effector function[33,36]; however, a notable therapeutic response was observed when used in combination with a tumor–specific antibody and systemic immune checkpoint blockade. In this work, we engineered an *E. coli* strain containing a synchronized lysis circuit (eSLC) that colonizes tumors and undergoes intratumoral quorum-lysis to locally release an encoded nanobody antagonist of CD47 (eSLC-CD47nb) (Fig. 1a). This system allows for the combined local delivery of an immunotherapeutic along with immunostimulatory bacterial lysis adjuvants to stimulate antitumor immunity and promote tumor regression.

To confirm expression and lysis-dependent release of CD47nb, we first transformed non-pathogenic *E. coli* with a single plasmid encoding the synchronized lysis circuit (eSLC), as well as a stabilized plasmid driving constitutive expression of a hemagglutinin (HA)-tagged variant of CD47nb (Extended Data Fig. 1). The SLC strain grows and produces the quorum-sensing molecule acylhomoserine lactone (AHL) via expression of *luxI*, then lyses at a critical threshold due to the production of a bacteriophage lysis protein (*ϕx174E*), resulting in bacterial death and therapeutic release[8] (Fig. 1a). Since this gene circuit was previously tested using two plasmids of differing copy numbers[8], we first assessed SLC-mediated lysis of eSLC-CD47nb *E.coli* by time-lapse microscopy of bacteria using an agar pad[37]. eSLC-CD47nb grew, reached quorum and lysed over a 20-hour time course, in contrast to non-SLC *E. coli* (SLC^-) which continuously grew and filled the field of view (Extended Data Fig. 2a). Furthermore, we cultured SLC^+ and SLC^- *E. coli* in LB broth in a 96-well plate and measured optical density (OD_{600}) over time. eSLC-CD47nb (SLC^+) exhibited multiple periodic dips in OD_{600}, indicating rounds of synchronized lysis, whereas SLC^- *E. coli* exhibited normal bacterial growth kinetics (Fig. 1b). Upon verifying synchronized lysis behavior, we evaluated the lysis-mediated release of CD47nb in batch cultures. Immunoblots

of log-phase bacterial cultures indicated that eSLC-CD47nb bacteria released significantly higher levels of HA-tagged CD47nb into culture supernatants than control CD47nb-HA bacteria without SLC (Extended Data Fig. 2b), suggesting that CD47nb release is enhanced by eSLC.

To verify that bacterially-produced nanobody functionally binds CD47, A20 murine lymphoma cells, known to express CD47[30], were incubated with a fixed concentration of FITC-labeled anti-mouse CD47 mAb (clone miap301) and varying dilutions of bacterial lysate from eSLC-CD47nb or eSLC expressing an empty vector (Fig. 1c and Extended Data Fig. 2c). We observed a progressive reduction in CD47 staining when cells were incubated with lysates from bacteria expressing CD47nb, suggesting that bacterially produced CD47nb could effectively outcompete miap301 binding to CD47 on the surface of A20 cells. We additionally cloned a C-terminal 6x-His tagged variant of CD47nb and purified recombinant CD47nb (rCD47nb) by Nickel-affinity chromatography. Similarly, we observed a progressive reduction in FITC fluorescence when A20 cells were co-incubated with increasing concentrations of rCD47nb and a fixed concentration of FITC-labeled miap301 (Extended Data Fig. 2d).

We also evaluated the ability of eSLC-CD47nb to induce A20 tumor cell phagocytosis by bone marrow–derived macrophages (BMDMs) (Fig. 1d, Extended Data Fig. 2e). As expected, treatment with anti-CD47 mAb resulted in a 60% increase in phagocytosis (Extended Data Fig. 2e) and treatment with eSLC lysate alone led to an increase in phagocytosis of tumor cells by 50%. Notably, eSLC-CD47nb treatment led to a 90% increase in phagocytosis compared to baseline, indicating that eSLC-CD47nb enhances phagocytosis of tumor cells by macrophages in a combinatorial, dose-dependent manner – via CD47 blockade and TLR agonism due to bacterial lysis adjuvants (Fig. 1d and Extended Data Fig. 2e). Overall, these results indicate that eSLC-CD47nb releases CD47nb in a lysis-dependent manner and that CD47nb can induce phagocytosis of tumor cells by BMDMs *in vitro*.

We next sought to evaluate the clinical efficacy of eSLC-CD47nb bacteria in a syngeneic mouse model. BALB/c mice were implanted with 5×10^6 A20 cells in both hind flanks. When tumors reached 100–150 mm^3 in volume, mice were randomly divided into three groups (PBS, eSLC, eSLC-CD47nb) and received intratumoral injections of PBS, or 10^7 colony forming units (CFU) of eSLC or eSLC-CD47nb bacteria resuspended in PBS, every 3–4 days for a total of 4 doses. While administration of control eSLC alone initially slowed tumor growth, likely due to the activation of innate immune cells by bacterial products released upon quorum-lysis, final tumor volumes were not statistically different from PBS treated mice. In contrast, administration of eSLC-CD47nb resulted in rapid and durable clearance of established A20 tumors within ~10 days of commencing therapy (Fig. 2a and Extended Data Figs. 3a and 3b). Importantly, unlike in animals receiving intratumoral injections of PBS or control eSLC bacteria, liver metastases were rarely observable in mice treated with eSLC-CD47nb at 30 days post-treatment (Fig. 2b). Of note, ~80% of mice treated with eSLC-CD47nb survived >90 days (Fig. 2c) and surviving mice were resistant to rechallenge by subcutaneous injection of 10×10^6 A20 cells (Fig. 2d), while naïve mice receiving the same batch of A20 cells developed tumors within a week of injection.

Subsequently, we explored the importance of therapeutic delivery by the individual components of our engineered, quorum-lysis system (Fig. 2e and Extended Data Fig. 3d). First, we evaluated efficacy of CD47 blockade via intraperitoneal delivery of anti-CD47 monoclonal antibody (miap301) with or without intratumoral injection of eSLC. Neither group demonstrated significant efficacy in comparison to treatment of eSLC alone in an A20 mouse model. While mice treated intratumorally with recombinant CD47nb (rCD47nb) or sonicated eSLC-CD47nb lysate exhibited slower tumor growth in comparison to mice treated with eSLC, complete tumor regression was only observed upon treatment with live, eSLC-CD47nb bacteria (Fig. 2e and Extended Data Fig. 3d). These data collectively suggest that continuous SLC-mediated intratumoral release of CD47nb is essential to therapeutic efficacy.

To assess the broader applicability of our approach, we also examined efficacy by intravenous administration, and using additional murine tumor models. Significant therapeutic efficacy was also observed when eSLC-CD47nb was intratumorally injected in other syngeneic murine models, such as triple negative breast cancer (4T1, Fig. 2f and Extended Data 4b) and melanoma (B16F10, Fig. 2h and Extended Data Fig. 4c). Lung metastases were notably reduced in mice receiving eSLC-CD47nb in the 4T1 triple-negative breast cancer model (Fig. 2g). We additionally explored the ability of eSLC-CD47nb to safely target and treat tumors via systemic intravenous delivery. In comparison to systemically delivered CD47 antibody (miap301), intravenous eSLC-CD47nb showed significantly slower tumor growth (Fig. 2i, Extended Data 5a). Following treatment, bacteria appeared to be exclusively localized within tumors as compared to the liver, spleen, and kidney (Extended Data Fig. 5b). Bacterial therapy was well-tolerated by animals, with no significant differences in body weight between treatment groups observed over the course of treatment or throughout the observation period by both intratumoral and intravenous delivery routes (Extended Data Figs. 3c, 4a and 5c). Overall, these results indicate that eSLC-CD47nb can safely promote local tumor regression while also preventing metastasis, suggesting the induction of systemic antitumor immunity that is likely mediated by tumor-specific T cells.

Recent studies have highlighted the importance of antigen presenting cells and effector T cells as being indispensable for anti-CD47–mediated clinical responses[30,31]. We reasoned that local inflammation induced by bacterial lysis coupled with localized blockade of CD47 on tumor cells would increase tumor cell phagocytosis and tumor antigen presentation, and thereby enhance the priming of antitumor T cells. Immunophenotyping of A20 tumors treated with eSLC-CD47nb revealed increased frequencies of $MHCII^{hi}$ $CD11b^{+}F4/80^{+}$ macrophages 3 days after commencing therapy (Extended Data Fig. 6a), suggesting an increase in the antigen presentation ability of tumor macrophages at early time points. Additionally, on day 8, we observed a decline in $SIRP\alpha^{+}$ macrophages within the tumor (Extended Data Fig. 6b). Past studies have shown that LPS exposure may lead to SIRPα downregulation *in vitro*[38]. We hypothesized that combined release of lysis adjuvants and a lack of SIRPα downstream signaling following CD47 blockade may lead to reduced surface expression of SIRPα on tumor-associated macrophages. Additionally, immunophenotyping of A20 tumors treated with eSLC-CD47nb revealed increased proliferation of both $Foxp3^{-}CD4^{+}$ and $CD8^{+}$ T cells (Fig. 3a and 3b) in comparison to tumor bearing mice

treated with eSLC bacteria. Furthermore, tumor-infiltrating Foxp3^{-}CD4^{+} T cells from eSLC-CD47nb-treated tumors produced significantly higher levels of IFN-γ following *ex vivo* restimulation with PMA and ionomycin (Fig. 3c). While we observed a trend towards higher IFN-γ levels in CD8^{+} T cells (Extended Data Fig. 6h), we observed markedly elevated levels of intratumoral Granzyme B^{+} CD8^{+} T cells (Fig. 3d) as well as other parameters of adaptive immune activation (Extended Data Figs. 6c–g). Additionally, these T cell responses appeared to be tumor antigen–specific as overnight *in vitro* co-culture of irradiated A20 cells with splenocytes derived from mice treated with eSLC-CD47nb led to robust secretion of IFN-γ (Extended Data Fig. 7). Interestingly, mice treated with miap301 exhibited no elevated IFN-γ response in comparison to those receiving eSLC-CD47nb. These data suggest that eSLC-CD47nb not only support the activation and proliferation of intratumoral T cells, but also lead to the induction of systemic antiA20 memory T cell responses.

Durable remission from cancer requires not only elimination of treated tumors but also systemic antitumor immunity for the clearance of distant metastases. Based on our observation that eSLC-CD47nb enhances the effector function of tumor-infiltrating T cells within treated tumors, we examined whether SLC-CD47nb could delay growth of untreated tumors. Mice injected with A20 tumors on both flanks were treated with eSLC-CD47nb in a unilateral fashion (Fig. 4a). While control eSLC bacteria had no effect on the growth of untreated tumors, treatment of the primary tumor with eSLC-CD47nb substantially slowed the growth of untreated tumors on the opposing flank (Fig. 4b and 4c, Extended Data Fig. 8a). To further quantify this effect, we computed the mean growth rates (mm/day) of treated vs. untreated tumors by calculating the slopes in tumor volume trajectories for each mouse (Fig. 4d). These data indicated that eSLC-CD47nb treated mice showed decreased growth rates in both treated and untreated tumors compared to controls. It has been shown that intratumorally released nanobody does not lead to systemic CD47 blockade[33], providing evidence that SLC-produced nanobody likely does not disseminate to the opposing, untreated tumor. However, we did consider the possibly that SLC-CD47nb bacteria injected into the primary tumor migrated via systemic circulation to seed the untreated lesion. We intratumorally injected a luminescent strain of SLC^{+} *E .coli* (EcNisLux[39]) into a single tumor and performed IVIS imaging over 5 days. In comparison to a SLC^{-} strain where luminescence continuously increased over time, SLC^{+} EcNisLux exhibited fluctuations in luminescence indicating *in vivo* lysis behavior (Extended Data Figs. 8 b, c). Importantly, luminescent signal was limited to the injected lesion and no signal was detected in the untreated tumor or other organs, indicating that an adaptive immune response may be mediating this abscopal effect. In support of this hypothesis, flow cytometric analysis of lymphocytes isolated from untreated tumors of mice whose primary tumors were injected with eSLC-CD47nb showed increased frequencies of activated (Extended Data Fig. 9e) and proliferating CD8^{+} T cells (Fig. 4e) as well as a trend towards increased frequencies of proliferating Foxp3^{-} CD4^{+} T cells (Extended Data Fig. 9a). Additionally, we observed a significantly higher percentage of Foxp3^{-} CD4^{+} and CD8^{+} T cells producing IFN-γ following *ex vivo* restimulation with PMA and ionomycin (Extended Data Figs. 9b, c). We directly assessed the reactivity of T cells in untreated tumors to an endogenous tumor antigen. Tumor-infiltrating lymphocytes were stimulated with an H-2Kd-restricted peptide

(A20-Id, DYWGQGTEL) corresponding to the unique idiotype of the antibody expressed by A20 lymphoma cells, which has previously been shown to activate tumor antigen–specific $CD8^+$ T cells[40]. Following *ex vivo* stimulation with A20-Id peptide, we observed a significantly higher frequency of $IFN\gamma^+$ $CD8^+$ T cells in mice treated with eSLC-CD47nb in comparison to mice treated with eSLC or PBS (Fig. 4f). As further confirmation of the specificity of this assay, we did not observe any changes in the frequency of $IFN\gamma^+$ $Foxp3^-$ $CD4^+$ T cells (Extended Data Fig. 9f) – consistent with this peptide being MHC class I restricted. These data suggest that treatment with eSLC-CD47nb enhances tumor antigen–specific $CD8^+$ T cell activity in the untreated tumor.

To further exclude the possibility of bacterial trafficking, we assessed the biodistribution of SLC^+ *E. coli* at 3 separate time points following unilateral intratumoral injection. Plating of homogenized tumors and organs revealed that bacterial growth remained restricted to treated tumors and no bacteria could be cultured from untreated tumors or livers and spleens of treated mice above the limit of detection (~1×10^3 CFU) (Fig. 4g). Additionally, SLC mediated release of CD47nb appeared to be necessary for inducing a potent abscopal effect. While eCD47nb (SLC^- strain constitutively producing CD47nb) administration slowed the growth of treated lesions in comparison to treatment with eSLC (Fig. 4h, Extended Data Fig. 10a), it exhibited a much weaker effect on untreated tumors in comparison to eSLC-CD47nb (Fig. 4i, Extended Data Fig. 10b). Taken together, these results clearly demonstrate that the engineered quorum-lysis immunotherapeutic delivery system can generate potent, tumor-specific adaptive immune responses that operate systemically to clear distant tumor lesions.

The approach described herein couples the inherently immunostimulatory nature of bacterial lysis products from programmable bacteria with potent nanobody-mediated blockade of an antiphagocytic receptor. Consequently, we observed enhanced infiltration and activation of tumor infiltrating lymphocytes leading to the induction of durable and systemic anti-tumor immunity. Our results suggest that localized, lysis-mediated release of anti-CD47 nanobody confers multiple advantages over conventional systemic monoclonal antibody therapy – firstly, intratumoral delivery of nanobody by eSLC increases the local concentration of immunotherapy while simultaneously preventing systemic toxicity. Second, local treatment with eSLC-CD47nb promotes the induction of systemic antitumor immune responses that are not observed following treatment with anti-CD47 monoclonal antibody. Finally, the ease of engineering bacteria to express additional immunotherapeutic nanobodies and/or cytokines, opens the possibility of evaluating combinations of several other immunotherapeutics which have exhibited systemic toxicity but may be safe and effective when delivered intratumorally using eSLC. The system we describe allows for the delivery of immunotherapeutics in a spatiotemporally defined manner and permits their delivery within diverse solid tumor settings. Moreover, due to the observed abscopal effect, this suggests a future strategy for treating metastatic lesions through the injection of accessible primary tumors.

METHODS

Strains and Plasmids

Plasmids were constructed using Gibson assembly or standard restriction enzyme–mediated cloning methods. The pSC01 SLC plasmid was constructed by first amplifying a region containing the constitutively expressed *luxR* gene and phage lysis gene, *ϕx174E* under the control of *luxI* promoter from a pZA35E plasmid[8]. Next, this was cloned into a pTD103-luxI plasmid[27] using the AvrII site. The pSC02 therapeutic plasmid was constructed by cloning a gBlock (IDT) encoding a *tac* promoter and an *E. coli* codon-optimized sequence for the A4 anti-CD47 nanobody[12] with an C-terminal hemagglutinin tag into the multiple cloning site of a pAH162 plasmid[41]. Additionally, two stabilizing elements, the hok/sok system[42] and alp7 partitioning system[43] were introduced into pSC02 to minimize plasmid loss *in vivo*. pSC01 and pSC02 were transformed into chemically competent *E. coli* $Pir1^+$ (Invitrogen). eSLC strains were grown in LB media with 50 μg/mL kanamycin (pSC01) and 100 μg/mL tetracycline (pSC02) along with 0.2% glucose at 37°C for under 12 hours in a shaking incubator. Glucose was added to reduce expression from the Lux promoter and prevent lysis *in vitro*. The pSC04 protein expression plasmid was constructed by cloning a gBlock (IDT) encoding an *E. coli* codon-optimized sequence for the A4 anti-CD47 nanobody[12] with a C-terminal 6x-Histidine tag into the multiple cloning site of an IPTG inducible pET vector under ampicillin resistance (100 μg/mL). pSC04 was transformed into NiCo21(DE3) *E. coli* (NEB).

Synchronized lysis circuit (SLC) characterization

To validate SLC function, SLC^+ and SLC^- *E. coli* were inoculated into LB media containing appropriate antibiotics and diluted 1:10. Samples were grown at 37°C in a round bottom 96 well plate in a shaking Tecan plate reader. OD_{600} was recorded every 10 minutes for 20 hours. Agar pads were prepared according to previous protocols[37]. SLC^+ and SLC^- *E. coli* were inoculated into LB media containing appropriate antibiotics and grown to mid-log phase. They were diluted 1:100 and grown under agar pads at 37°C and imaged using a Nikon Ti-E microscope equipped with an Okolab stage top incubator.

Bacterial nanobody characterization

For purification of recombinant CD47nb (rCD47nb), pSC04 containing NiCo21(DE3) *E. coli* were grown at 37 °C to ~0.8 OD_{600} and induced with 1 mM IPTG for 20h at 30 °C. Cells were centrifuged at 4000 rpm for 10 min. After resuspension in lysis buffer (50 mM NaH_2PO_4, 300 mM NaCl, pH 8.0) and sonication, lysates were spun at 10000 rpm for 30 min at 4 °C. The supernatant was loaded on to Ni-NTA (Qiagen) resin and washed in wash buffer (35 mM imidazole) followed by elution in 250 mM imidazole. The elutions were then dialyzed in PBS using regenerated cellulose dialysis tubing (3500 Da MWCO), and the solution was filtered through a 0.2 μm filter to remove any residual debris and stored at −80 °C.

Overnight cultures of *E. coli* containing pSC01 and pSC02 were grown in appropriate antibiotics and 0.2% glucose. A 1:100 dilution into LB with antibiotics was made the following day and bacteria were grown in a shaking incubator at 37°C. Optical Density

(OD) was measured every 30 mins until the OD of lysing strains began to fall, indicating lysis. At this point OD normalized bacteria were spun down at 3000 rcf and supernatants were filtered through a 0.2 μm filter. Cell pellets were mechanically lysed by 3–4 freeze-thaw cycles. Supernatants and lysates were separated by SDS-PAGE followed by immunoblotting with rat anti-HA (Sigma) antibody to evaluate the presence of recombinant CD47nb (rCD47nb) protein in culture fractions. To verify binding of bacterially produced nanobody to CD47 on tumor cells, serial dilutions of bacterial supernatants from SLC bacteria with or without pSC02 or rCD47nb were co-incubated with FITC-labeled anti-CD47 antibody in the presence of A20 tumor cells for 1 hour and FITC fluorescence was measured by flow cytometry.

in vitro phagocytosis

Overnight cultures of *E. coli* containing pSC01 and pSC02 were grown in appropriate antibiotics and 0.2% glucose. A 1:100 dilution into LB with antibiotics was made the following day and bacteria were grown to mid-log phase in a shaking incubator at 37°C. Bacteria were pelleted at 3000 rcf and lysed by sonication. To obtain eSLC and eSLC-CD47nb lysates, sonicates were spun at 10000 rpm for 5 min and supernatants were filtered through a 0.2 μm filter to remove any residual debris. Harvested bone marrow–derived macrophages (BMDMs) were detatched and seeded on to a transparent 96-well tissue culture plate at 5×10^4 cells per well. A20 tumor cells were incubated for 10 min with 5 μM Vybrant DiI solution (Invitrogen). Labeled A20 cells were pre-treated with serial dilutions of bacterial lysates (eSLC or eSLC-CD47nb) or with anti-CD47 mAb, isotype or PBS. Following 3.5 h coincubation of labeled, pre-treated A20 cells and BMDMs, residual A20 cells were washed and BMDMs were stained with NucBlue. Multiple random fields were imaged for each replicate using a Nikon Ti-E microscope. The ratio of DiI^+ BMDMs to total $NucBlue^+$ BMDMs was counted for each field to score phagocytosis.

Animal models

All animal experiments were approved by the Institutional Animal Care and Use Committee (Columbia University, protocol AC-AAAN8002 and AC-AAAZ4470). The protocol requires animals to be euthanized when tumor burden reaches 2 cm in diameter or under veterinary staff recommendation. Mice were blindly randomized into various groups. Animal experiments were performed on 4–8 week-old female BALB/c mice or C57BL/6 (Taconic Biosciences) with bilateral subcutaneous hind flank tumors from A20 murine lymphoma cells (ATCC), 4T1-luciferase mammary carcinoma cells (ATCC, luciferized by stable plasmid transfection), or B16-F10 melanoma cells. Cells were injected subcutaneously at a volume of 100 μl per flank, with each implant consisting of 5×10^6 cells (BALB/c, A20), 10^6 cells (BALBc, 4T1), or 5×10^5 (C57BL/6, B16-F10). Tumors were grown to an average volume of approximately 100–200 mm^3 before treatment with bacterial strains. Tumor volume was calculated by measuring the length and width of each tumor using calipers, where $V = \text{length} \times \text{width}^2 \times 0.5$ as previously calculated[30]. For all tumor growth experiments, a minimum of 4 mice per group were used. The growth in mm/day was computed by taking the difference between tumor volumes at adjacent time points for a particular animal. Values were computed as the mean with standard error plotted.

Bacterial administration for *in vivo* experiments

Bacterial strains were grown overnight in LB media containing appropriate antibiotics and 0.2% glucose. A 1:100 dilution into media with antibiotics was started the day of injection and grown to an OD_{600} of approximately 0.1. Bacteria were spun down and washed 3 times with sterile PBS before injection into mice. Intratumoral injections of bacteria were performed at a concentration of 5×10^8 CFU per ml in PBS with a total volume of 20–40 μl injected per tumor. Tail-vein (intravenous) injections of bacteria were performed at a concentration of 5×10^7 CFU per ml in PBS with a total volume of 100 μl injected per mouse.

Biodistribution and *in vivo* bacterial dynamics

Following treatment with 10^7 SLC^+ *E. coli*, tumors, spleen and liver were weighed and homogenized using a gentleMACS tissue dissociator (Miltenyi Biotec) (C-tubes). Homogenates were serially diluted and plated on LB-agar plates at 37°C overnight. Colonies were counted (limit-of-detection 10^3 CFU/g) and computed as CFU/g of tissue. To determine *in vivo* dynamics of SLC^+ and SLC^- *E. coli*, 10^7 SLC^+ or SLC^- *E. coli Nislux* (genomic expression of luxCDABE cassette) were injected unilaterally into hind-flank tumors. Luminescent signal was measured at multiple time-points over 4 days with an *In vivo* imaging system (IVIS) following bacterial injection to follow dynamics.

Flow cytometry

Tumors were extracted for immunophenotyping on day 3 or day 8 following commencement of bacterial therapy. Myeloid and lymphoid subsets were isolated from tumor tissue by mechanical homogenization of tumor tissue followed and digestion with collagenase A (1 mg/ml; Roche) and DNase I (0.5 μg/ml; Roche) in isolation buffer (RPMI 1640 supplemented with 5% FBS, 1% l-glutamine, 1% pen-strep and 10 mM Hepes) for 1 hour at 37°C. Cells were filtered through 100 μm cell strainers, washed in isolation buffer and stained. Dead cells were excluded by staining with Ghost Dye cell viability reagent. Extracellular antibodies used included anti-B220 (BD), anti-CD4 (Tonbo), anti-CD8 (eBioscience) anti-NKp46 (BD), anti-Gr-1 (Tonbo) anti-CD11b (BD), anti-F4/80 (eBioscience) anti-SIRPα (BioLegend) and anti-MHC Class II (Tonbo). To measure T cell production of cytokines, cells were stimulated for 2 hours with PMA (50 ng/ml Sigma), ionomycin (1nM; Calbiochem) in the presence of GolgiPlug (brefeldin A). To measure tumor antigen-specific T cell production of cytokines, cells were stimulated for 5 hours with A20-Id (DYWGQGTEL) peptide (GenScript) for 5 hours in the presence of GlogiPlug (brefeldin A). Following extracellular staining with the aforementioned antibodies, intracellular staining was performed using anti-CD3 (Tonbo) anti-TCRβ (BD), anti-CTLA4 (eBioscience), anti-Foxp3 (eBioscience), anti-Ki-67 (Thermo), anti-Granzyme-B (Biolegend) and cytokines (anti-IL-17 (eBioscience), anti-TNF-α (eBioscience), anti-IFN-γ (Tonbo). Cells were fixed using Foxp3/transcription factor staining buffer set (Tonbo) as per manufacturer's protocol. Samples were analyzed using a BD LSRFortessa cell analyzer.

Statistical analysis

Statistical tests were calculated in GraphPad Prism v7.0 and v8.0. The details of the statistical tests carried out are indicated in the respective figure legends. Where data were approximately normally distributed, values were compared using either a Student's *t*-test or one-way ANOVA for single variable, or a two-way ANOVA for two variables with Tukey's correction for multiple comparisons. For Kaplan-Meier survival experiments we performed a Log-rank (Mantel-Cox) test. Mice were randomized in different groups before experiments.

Data availability

The data that support the findings of this study are available within the paper and its supplementary information files. Additional data are available from the authors upon reasonable request.

Extended Data

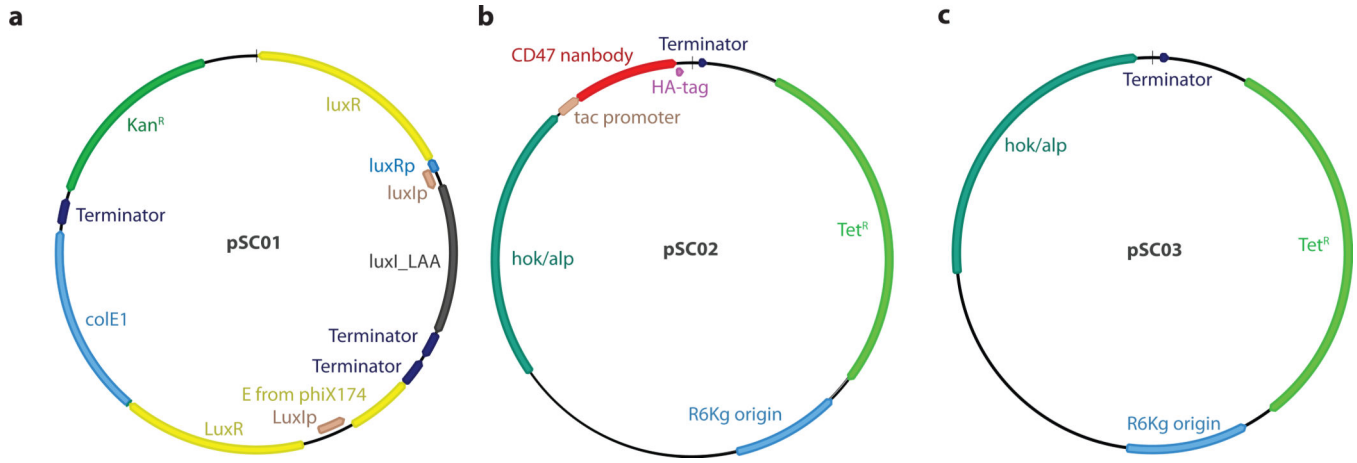

Extended Data Figure 1 |. Map of plasmids used in this study.

a, pSC01, single plasmid synchronized lysis circuit. **b**, pSC02, stabilized plasmid driving constitutive expression of HA-tagged anti-CD47 nanobody. **c**, pSC03 empty vector control.

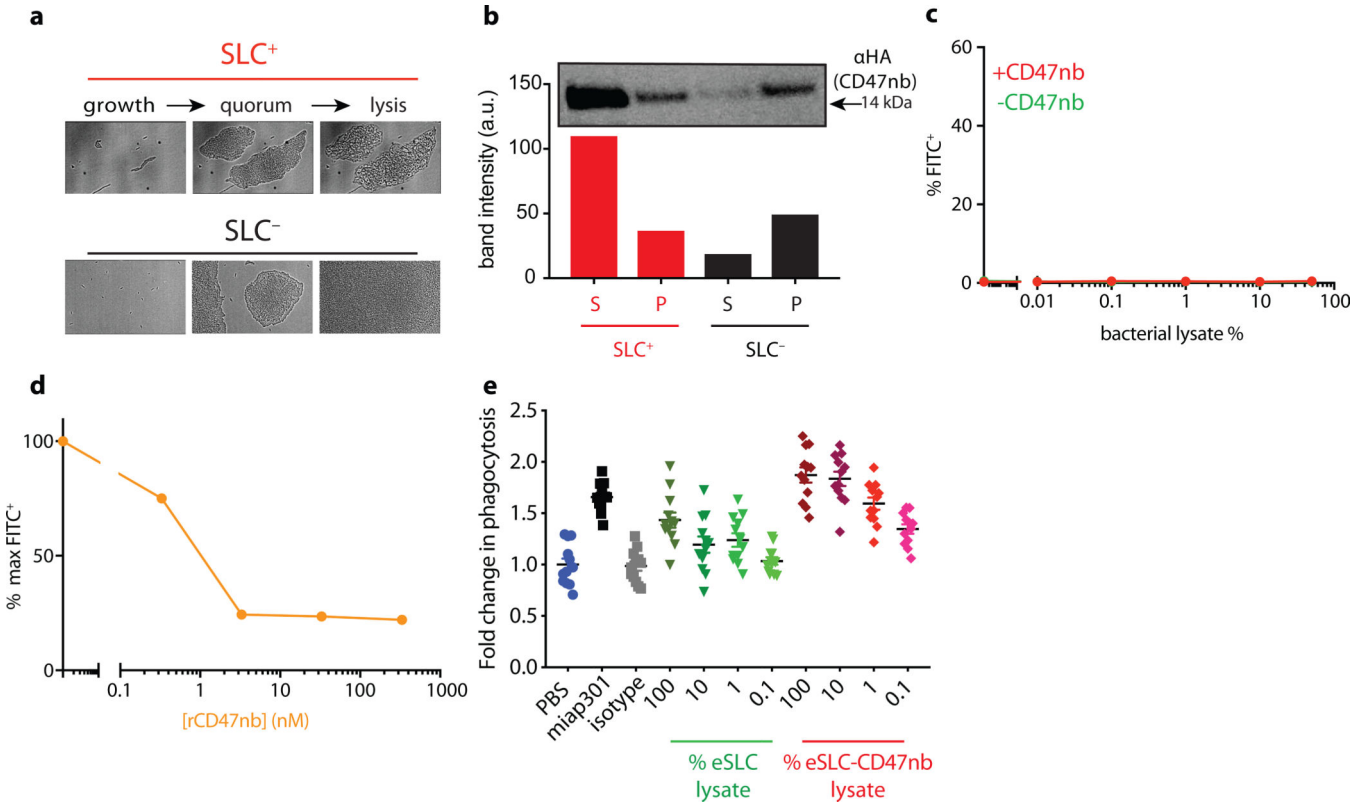

Extended Data Figure 2 |. *E. coli* capable of synchronized lysis produce functional anti-CD47 nanobody.

a, Bacterial growth dynamics over time in agar-pad microscope experiments. **b,** Immunoblot of bacterial culture supernatants (S) and cell pellets (P) in strains with and without SLC designed to constitutively produce HA-tagged CD47 nanobody. **c,** A20 cells were co-incubated with a fixed concentration of FITC conjugated IgG2a-FITC isotype control along with varying concentrations of bacterial lysates containing constitutively expressed CD47nb or empty vector. **d**, A20 cells were co-incubated with a fixed concentration of FITC-conjugated anti-CD47 (miap301) antibody along with serial dilutions of recombinant 6xHis-tagged CD47nb (rCD47nb). **e**, *in vitro* phagocytosis of DiI labeled A20 cells pretreated with PBS, miap301, IgG2a isotype control, or serial dilutions of eSLC or eSLC-CD47nb lysate in PBS by bone-marrow derived macrophages.

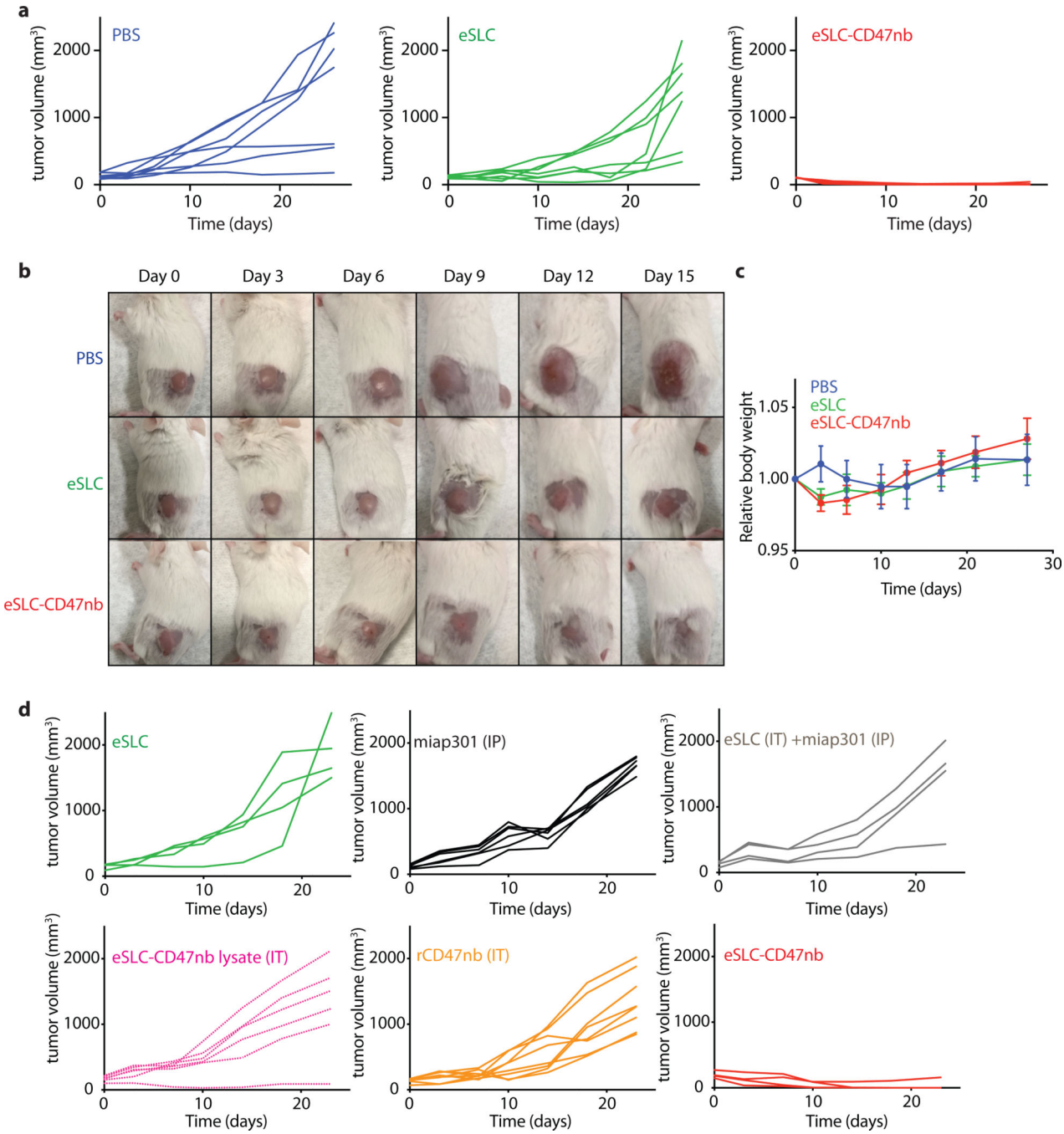

Extended Data Figure 3 |. Individual kinetics of intratumoral bacterial immunotherapy.
a, Individual tumor growth trajectories (n=7 per group). **b,** Representative images of subcutaneous A20 tumor bearing BALB/c mice treated with PBS, eSLC, or eSLC-CD47nb. **c**, Relative body weight of A20 tumor bearing BALB/c mice over time (ns (not significant), two-way ANOVA with Tukey's multiple comparisons test). **d,** Individual tumor growth trajectories (n=4–8 per group) following treatment with eSLC (IT), miap301 (IP), eSLC (IT) + miap301 (IP), eSLC-CD47nb lysate, rCD47nb (IT) or eSLC-CD47nb (IT).

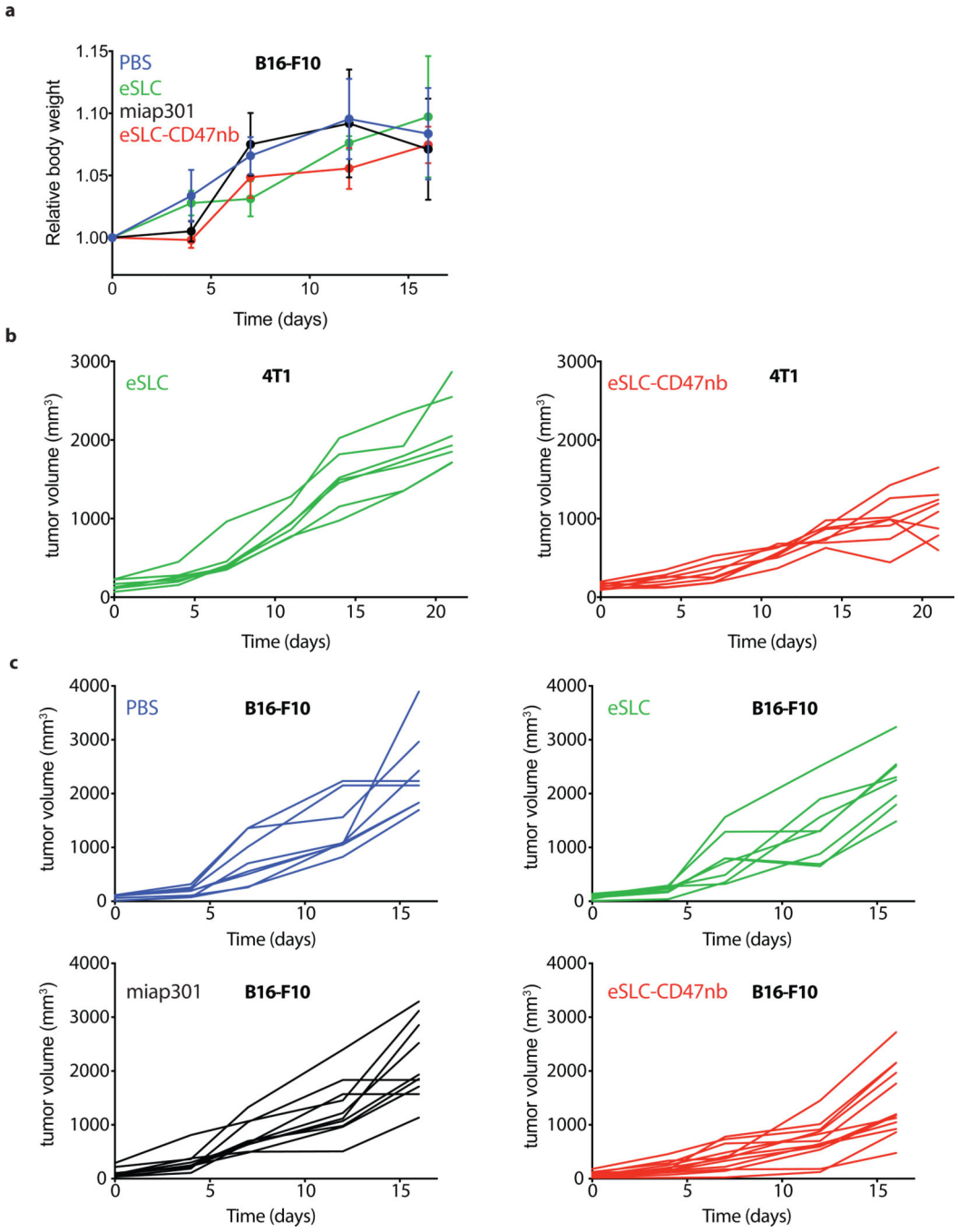

Extended Data Figure 4 |. Immunotherapeutic bacteria limit tumor growth in syngeneic murine models of melanoma and triple negative breast cancer.

a, Relative body weight of B16-F10 bearing C57BL/6 mice over time (n=4–5 mice per group, ns, two-way ANOVA with Tukey's multiple comparisons test) **b**, Individual tumor growth trajectories of subcutaneous 4T1 tumors following intratumoral eSLC or eSLC-CD47nb injection (n=6–8 per group). **c**, Individual tumor growth trajectories of subcutaneous B16-F10 melanoma following intraperitoneal miap301 or intratumoral PBS, eSLC, or eSLC-CD47nb injection (n=8–12 per group).

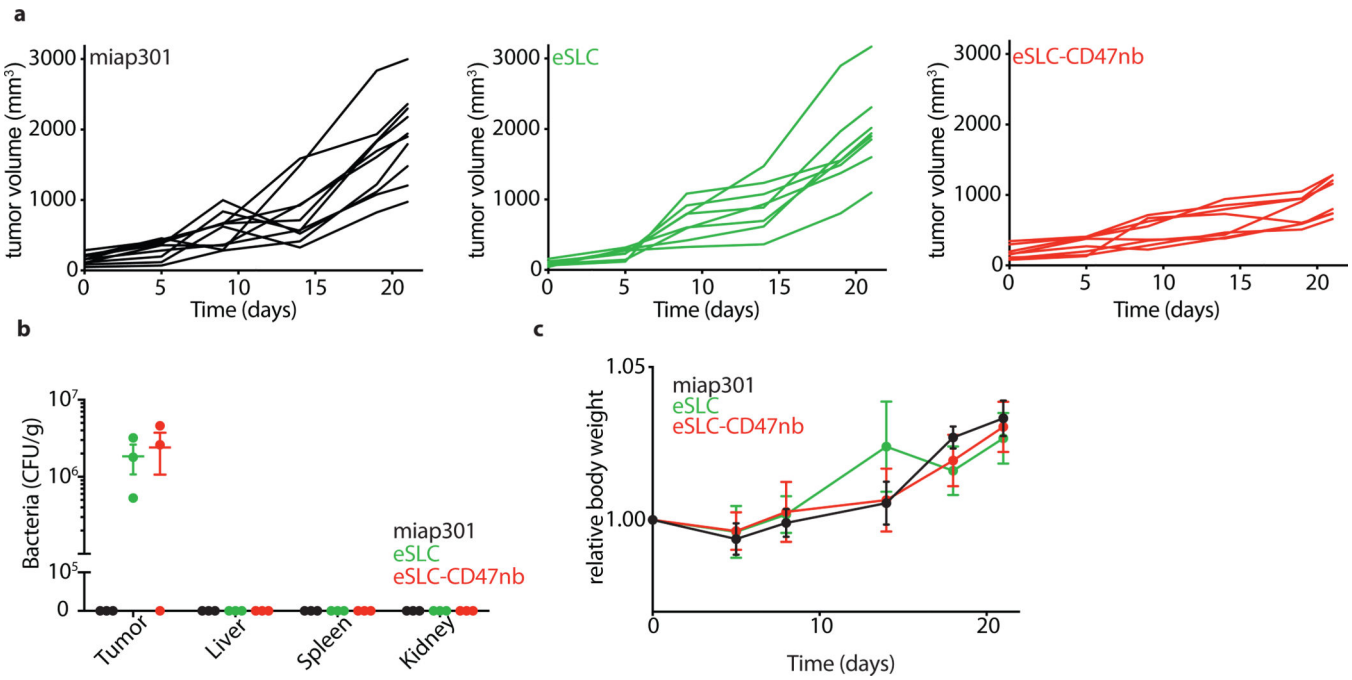

Extended Data Figure 5 |. Intravenous bacterial immunotherapy limits tumor growth in a subcutaneous A20 lymphoma model.

a, Individual tumor growth trajectories of subcutaneous A20 tumors following intraperitoneal miap301 or intravenous eSLC or eSLC-CD47nb treatment (n=8–10 per group). **b,** Biodistribution of eSLC-CD47nb *E. coli* on day 8 following final intravenous bacterial treatment. Excised tumors, livers, spleens and kidneys were homogenized, serially diluted and plated on LB agar plates. Colonies were counted to determine CFU/g of tissue (n=3 per group). **c**, Relative body weight of A20 tumor bearing BALB/c mice receiving intravenous bacterial injections or intraperitoneal injections of miap301 (n=4–5 per group, ns, two-way ANOVA with Tukey's multiple comparisons test).

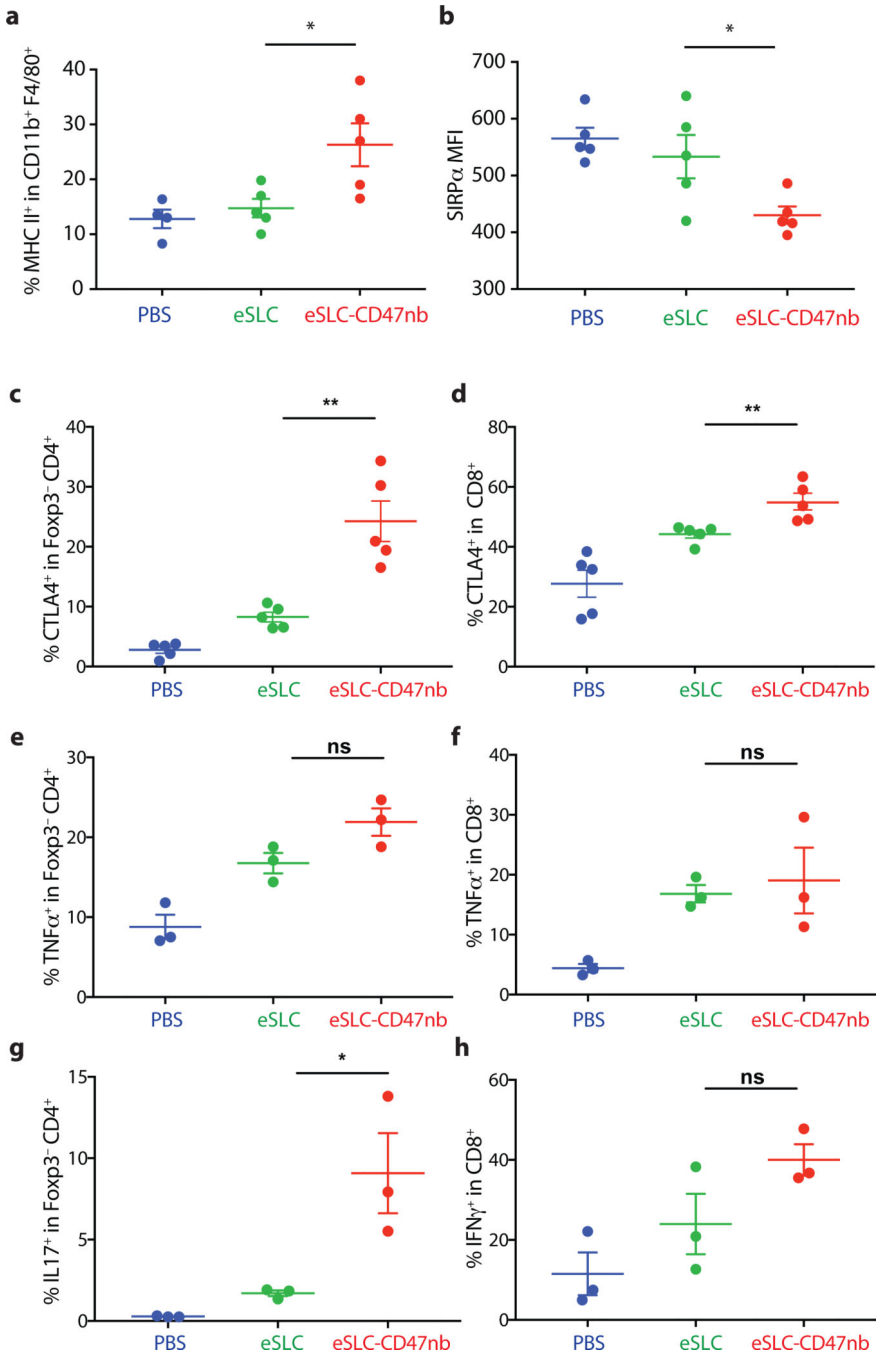

Extended Data Figure 6 |. Immunophenotyping of tumor infiltrating myeloid and lymphoid subsets following intratumoral bacterial injection.

5×10^6 A20 cells were subcutaneously implanted into the hind flanks of BALB/c mice. When tumors reached 100–150 mm^3 in volume (day 0), mice were treated with either PBS, eSLC or eSLC-CD47nb on days 0, 4 and 7. On day 3 or day 8, tumors were homogenized and tumor-infiltrating myeloid and lymphoid subsets were isolated for flow cytometric analysis (n=3–5 mice per group) **a,** Frequency of isolated MHC II^{hi} $CD11b^+$ $F4/80^+$ macrophages on day 3 following treatment. **b**, MFI of SIRPα staining within $CD11b^+$

F4/80$^+$ subset on day 8 following treatment. **c, d,** Frequencies of CTLA4$^+$ within Foxp3$^-$CD4$^+$ and CD8$^+$ T cells, respectively. **e, f,** Frequencies of TNFα$^+$ within Foxp3$^-$CD4$^+$ and CD8$^+$ T cells, respectively following *ex vivo* stimulation. **g,** Frequency of IL17$^+$ within Foxp3$^-$CD4$^+$ T cells following *ex vivo* stimulation. **h,** Frequency of IFNγ$^+$ within CD8$^+$ T cells following *ex vivo* stimulation. (*P<0.05, **P<0.01, unpaired t-test)

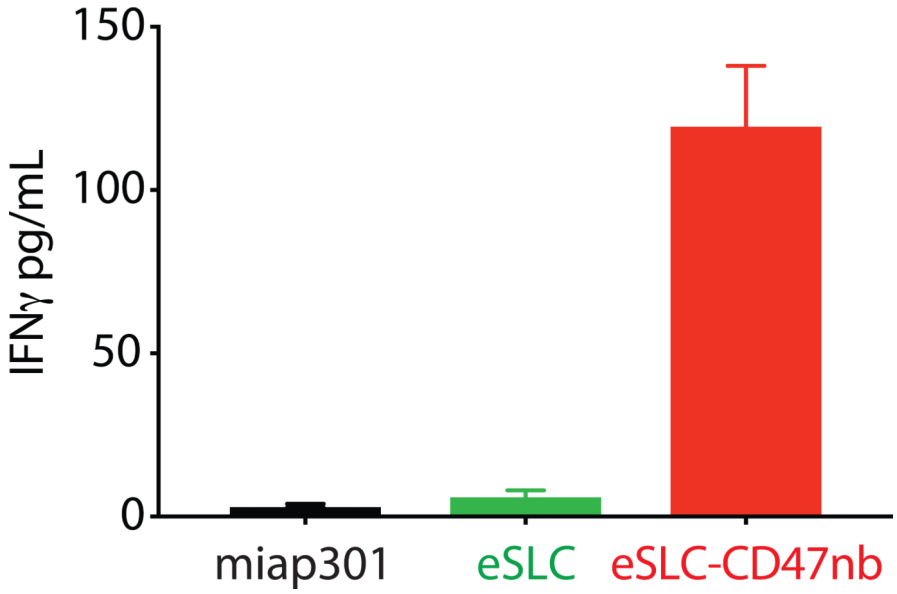

Extended Data Figure 7 |. Immunotherapeutic bacteria lead to increased interferon-γ production by splenic T cells following stimulation with tumor antigens.

IFN-γ ELISA of supernatants from overnight coincubation of splenocytes isolated from each of the indicated treatment groups with irradiated A20 cells (n=2 mice per group, 3 technical replicates).

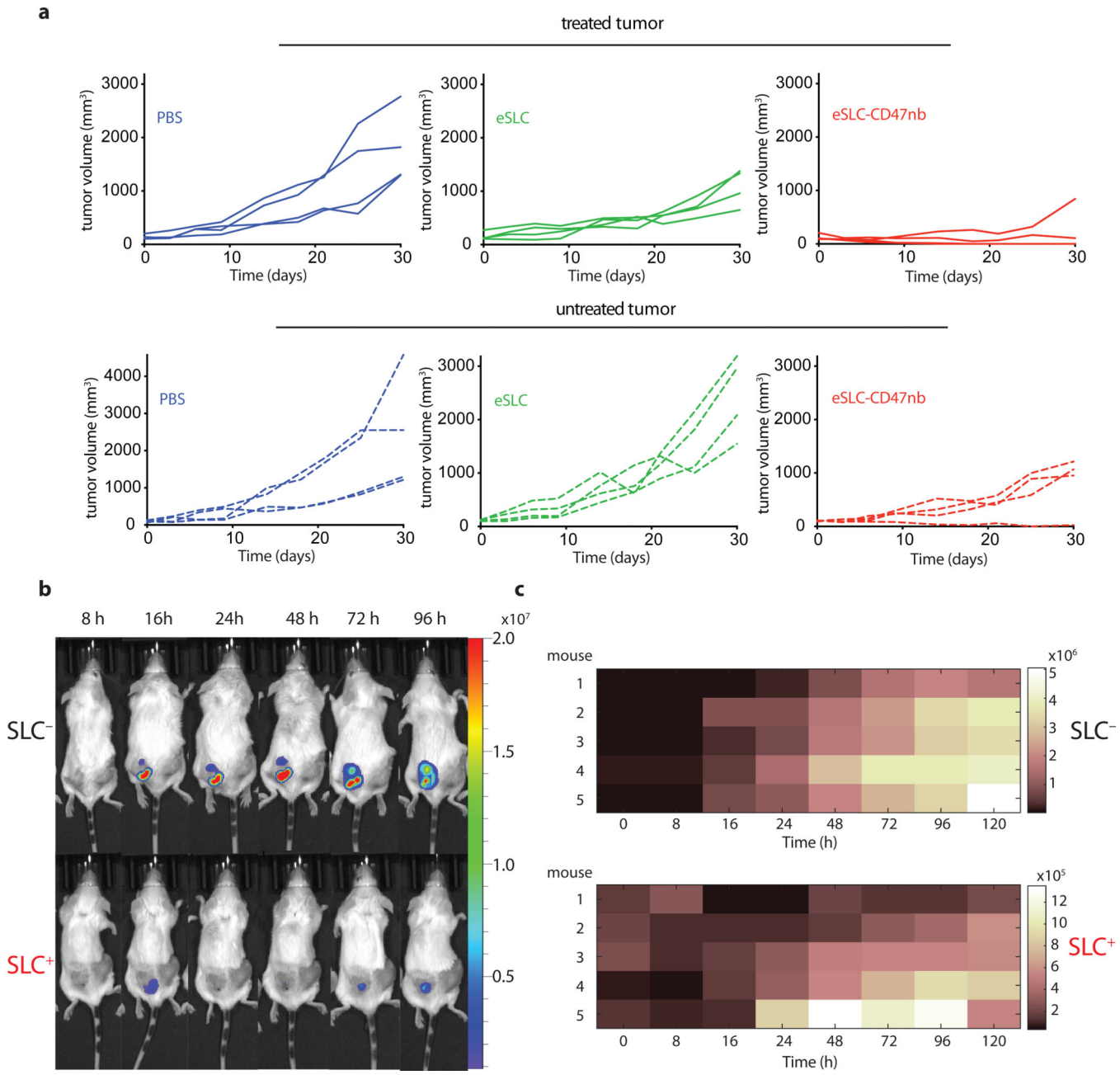

Extended Data Figure 8 |. Intratumoral bacterial immunotherapy leads to distal tumor control.
a, Individual tumor growth trajectories of treated (injected) and untreated A20 tumors following intratumoral PBS, eSLC, or eSLC-CD47nb injection. **b**, SLC^- and SLC^+ EcNisLux were intratumorally injected into a single-flank of A20 tumor bearing mice (scale represents radiance (p/s/cm2/sr). Luminescence was measured over time via IVIS. Representative image of mouse #3 from each group over time. **c**, Luminescence heat maps over time (n=5 mice per group). Colors represent average radiance (p/s/cm2/sr).

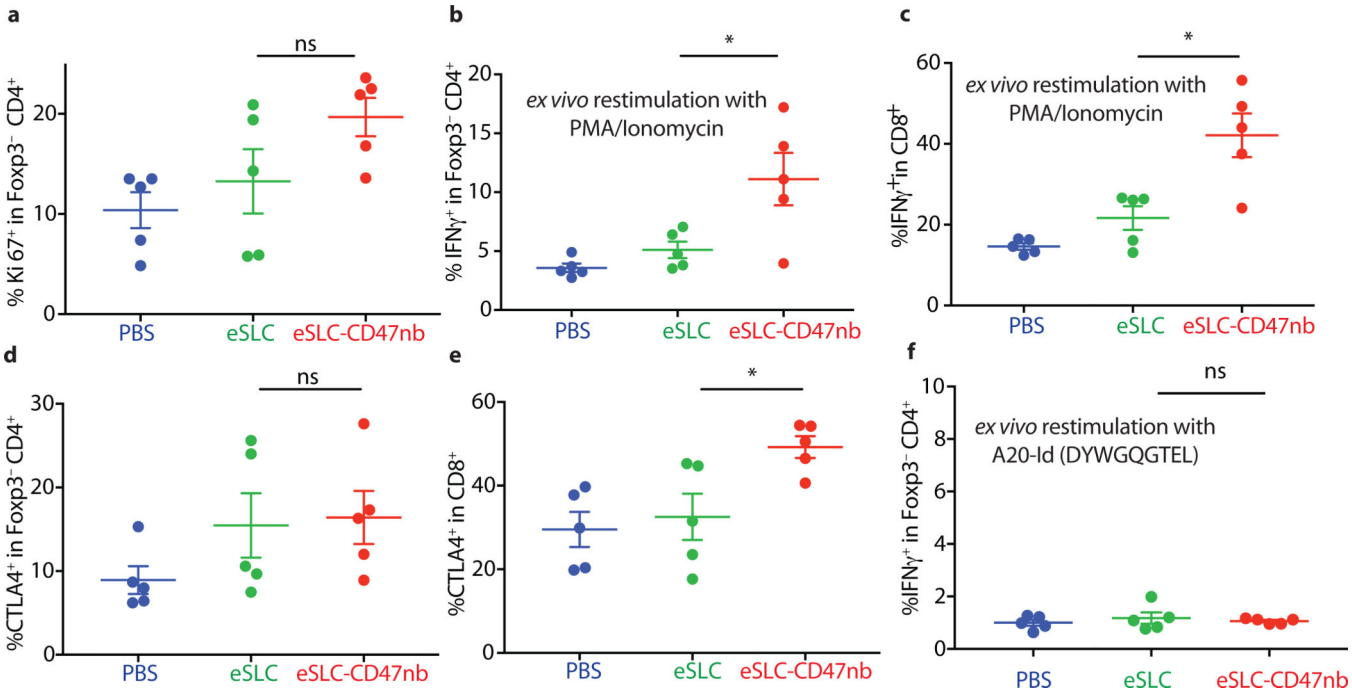

Extended Data Figure 9 |. Immunophenotyping of tumor infiltrating lymphocytes in untreated tumors following single-flank bacterial injection.

5×10^6 A20 cells were implanted into the hind flanks of BALB/c mice. When tumors reached ~100 mm^3 in volume (day 0), mice were treated with either PBS, eSLC or eSLC-CD47nb on day 0, 4 and 7 into a single tumor. Untreated tumors were extracted and analyzed by flow cytometry on day 8. n=5 mice per group. **a,** Frequency of Ki-67$^+$ cells within Foxp3$^-$CD4$^+$ T cells (ns, unpaired t-test). **b**, **c,** Frequency of tumor infiltrating IFNγ^+ within Foxp3$^-$CD4$^+$ T cells and CD8$^+$ T cells respectively following *ex vivo* stimulation with PMA and ionomycin in the presence of brefeldin A (*, P<0.05, unpaired t-test). **d, e**, Frequencies of CTLA4$^+$ within Foxp3$^-$CD4$^+$ T and CD8$^+$ T cells compartments, respectively. (* P<0.05, unpaired t-test). f, Frequency of tumor infiltrating IFNγ^+ within Foxp3$^-$ CD4$^+$ T cells following ex vivo restimulation with A20-Id peptide (DYWGQGTEL) in the presence of brefeldin A (ns, unpaired t-test).

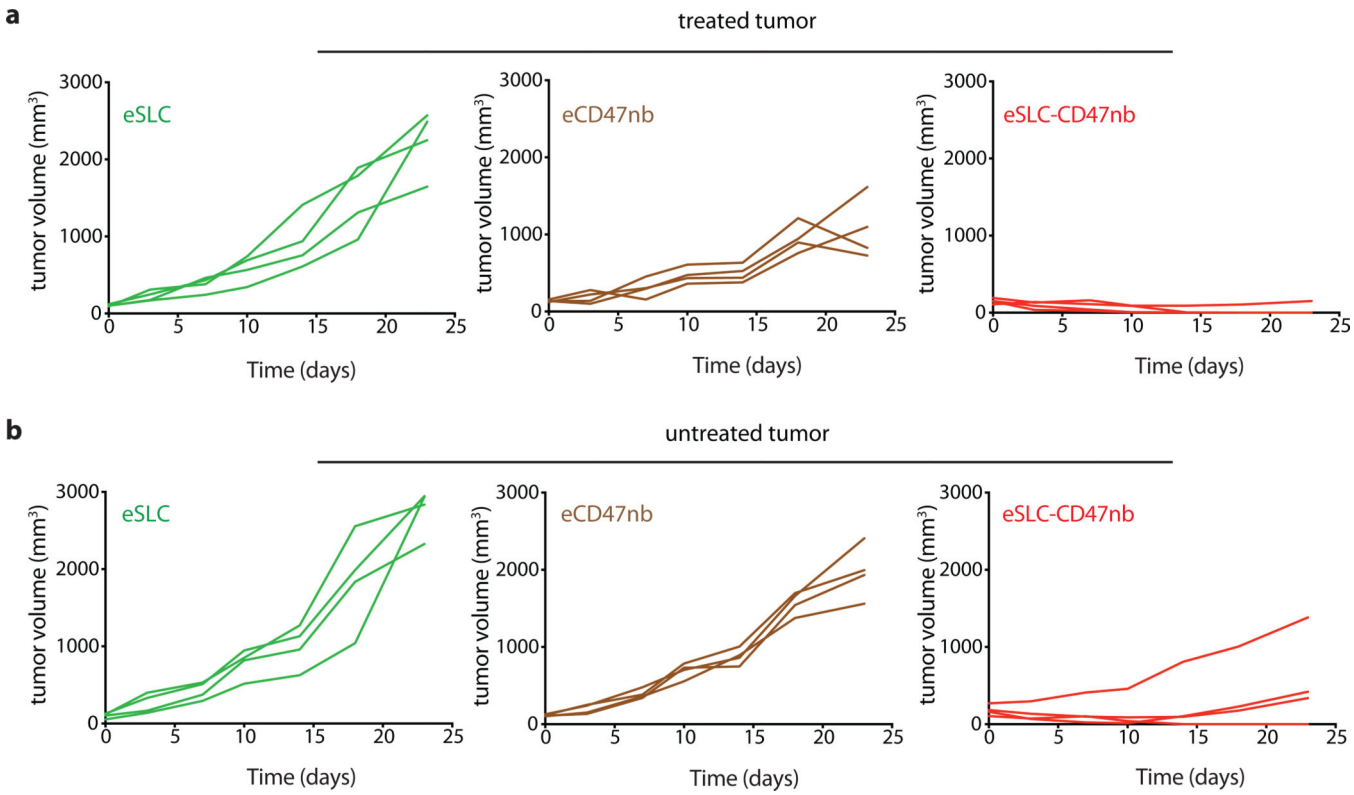

Extended Data Figure 10 |. Distal tumor control requires SLC$^+$ bacteria engineered to produce CD47nb.

a, **b**, Individual tumor growth trajectories of treated (injected) and untreated A20 tumors following intratumoral eSLC, eCD47nb, or eSLC-CD47nb injection (n=4 mice per group).

ACKNOWLEDGEMENTS

This work was supported by the NIH Pathway to Independence Award (R00CA197649-02) (T.D.), DoD Idea Development Award (LC160314) (T.D.), DoD Era of Hope Scholar Award (BC160541) (T.D.), NIH AI127847 (N.A.), Searle Scholars Program SSP-2017-2179 (N.A.), and the Roy and Diana Vagelos Precision Medicine Pilot Grant (N.A. and T.D.). Research reported in this publication was performed in the Columbia University Department of Microbiology & Immunology Flow Cytometry Core facility. The content is solely the responsibility of the authors and does not necessarily represent the official views of the National Institutes of Health. We would like to thank Katherine T. Fortson and Oscar Velasquez for technical assistance with flow cytometry experiments and *in vivo* tumor experiments respectively. We would like to thank M. Omar Din for input pertaining to SLC characterization experiments. We would like to thank Vivian Yeong and members of the Obermeyer group for assistance with affinity-chromatography and protein purification. We thank Rosa L. Vincent, Thomas M. Savage, Katherine A. Kaiser and Lucas F. Loffredo for review of the manuscript.

REFERENCES

1. Fischbach MA, Bluestone JA & Lim WA Cell-based therapeutics: the next pillar of medicine. Sci Transl Med 5, 179ps177 (2013).
2. Weber W & Fussenegger M Emerging biomedical applications of synthetic biology. Nat Rev Genet 13, 21–35 (2011). [PubMed: 22124480]
3. Lim WA & June CH The Principles of Engineering Immune Cells to Treat Cancer. Cell 168, 724–740 (2017). [PubMed: 28187291]
4. Ruder WC, Lu T & Collins JJ Synthetic biology moving into the clinic. Science 333, 1248–1252 (2011). [PubMed: 21885773]

5. Chen YY & Smolke CD From DNA to targeted therapeutics: bringing synthetic biology to the clinic. Sci Transl Med 3, 106ps142 (2011).
6. Wu MR, Jusiak B & Lu TK Engineering advanced cancer therapies with synthetic biology. Nat Rev Cancer (2019).
7. Chien T, Doshi A & Danino T Advances in bacterial cancer therapies using synthetic biology. Curr Opin Syst Biol 5, 1–8 (2017). [PubMed: 29881788]
8. Din MO, et al. Synchronized cycles of bacterial lysis for in vivo delivery. Nature 536, 81–85 (2016). [PubMed: 27437587]
9. Pedrolli DB, et al. Engineering Microbial Living Therapeutics: The Synthetic Biology Toolbox. Trends Biotechnol (2018).
10. Zhou S, Gravekamp C, Bermudes D & Liu K Tumour-targeting bacteria engineered to fight cancer. Nat Rev Cancer 18, 727–743 (2018). [PubMed: 30405213]
11. Helmink BA, Khan MAW, Hermann A, Gopalakrishnan V & Wargo JA The microbiome, cancer, and cancer therapy. Nat Med 25, 377–388 (2019). [PubMed: 30842679]
12. Sockolosky JT, et al. Durable antitumor responses to CD47 blockade require adaptive immune stimulation. Proc Natl Acad Sci U S A 113, E2646–2654 (2016). [PubMed: 27091975]
13. Majeti R, et al. CD47 is an adverse prognostic factor and therapeutic antibody target on human acute myeloid leukemia stem cells. Cell 138, 286–299 (2009). [PubMed: 19632179]
14. Willingham SB, et al. The CD47-signal regulatory protein alpha (SIRPa) interaction is a therapeutic target for human solid tumors. Proc Natl Acad Sci U S A 109, 6662–6667 (2012). [PubMed: 22451913]
15. Coley WB II. Contribution to the Knowledge of Sarcoma. Ann Surg 14, 199–220 (1891).
16. Berendt MJ, North RJ & Kirstein DP The immunological basis of endotoxin-induced tumor regression. Requirement for T-cell-mediated immunity. J Exp Med 148, 1550–1559 (1978). [PubMed: 309921]
17. Tsung K & Norton JA Lessons from Coley's Toxin. Surg Oncol 15, 25–28 (2006). [PubMed: 16814541]
18. Mellman I, Coukos G & Dranoff G Cancer immunotherapy comes of age. Nature 480, 480–489 (2011). [PubMed: 22193102]
19. Jiang SN, et al. Inhibition of tumor growth and metastasis by a combination of Escherichia coli-mediated cytolytic therapy and radiotherapy. Mol Ther 18, 635–642 (2010). [PubMed: 20051939]
20. Malmgren RA & Flanigan CC Localization of the vegetative form of Clostridium tetani in mouse tumors following intravenous spore administration. Cancer Res 15, 473–478 (1955). [PubMed: 13240693]
21. Brown JM & Wilson WR Exploiting tumour hypoxia in cancer treatment. Nat Rev Cancer 4, 437–447 (2004). [PubMed: 15170446]
22. Forbes NS Engineering the perfect (bacterial) cancer therapy. Nat Rev Cancer 10, 785–794 (2010). [PubMed: 20944664]
23. Zheng JH, et al. Two-step enhanced cancer immunotherapy with engineered Salmonella typhimurium secreting heterologous flagellin. Sci Transl Med 9(2017).
24. Gardner TS, Cantor CR & Collins JJ Construction of a genetic toggle switch in Escherichia coli. Nature 403, 339–342 (2000). [PubMed: 10659857]
25. Basu S, Gerchman Y, Collins CH, Arnold FH & Weiss R A synthetic multicellular system for programmed pattern formation. Nature 434, 1130–1134 (2005). [PubMed: 15858574]
26. Friedland AE, et al. Synthetic gene networks that count. Science 324, 1199–1202 (2009). [PubMed: 19478183]
27. Danino T, Mondragon-Palomino O, Tsimring L & Hasty J A synchronized quorum of genetic clocks. Nature 463, 326–330 (2010). [PubMed: 20090747]
28. Elowitz MB & Leibler S A synthetic oscillatory network of transcriptional regulators. Nature 403, 335–338 (2000). [PubMed: 10659856]
29. Jaiswal S, et al. CD47 is upregulated on circulating hematopoietic stem cells and leukemia cells to avoid phagocytosis. Cell 138, 271–285 (2009). [PubMed: 19632178]

30. Liu X, et al. CD47 blockade triggers T cell-mediated destruction of immunogenic tumors. Nat Med 21, 1209–1215 (2015). [PubMed: 26322579]
31. Kauder SE, et al. ALX148 blocks CD47 and enhances innate and adaptive antitumor immunity with a favorable safety profile. PloS one 13, e0201832 (2018). [PubMed: 30133535]
32. Liu X, et al. Dual Targeting of Innate and Adaptive Checkpoints on Tumor Cells Limits Immune Evasion. Cell Rep 24, 2101–2111 (2018). [PubMed: 30134171]
33. Ingram JR, et al. Localized CD47 blockade enhances immunotherapy for murine melanoma. Proc Natl Acad Sci U S A 114, 10184–10189 (2017). [PubMed: 28874561]
34. Huang Y, Ma Y, Gao P & Yao Z Targeting CD47: the achievements and concerns of current studies on cancer immunotherapy. J Thorac Dis 9, E168–E174 (2017). [PubMed: 28275508]
35. Advani R, et al. CD47 Blockade by Hu5F9-G4 and Rituximab in Non-Hodgkin's Lymphoma. N Engl J Med 379, 1711–1721 (2018). [PubMed: 30380386]
36. Veillette A & Chen J SIRPalpha-CD47 Immune Checkpoint Blockade in Anticancer Therapy. Trends Immunol 39, 173–184 (2018). [PubMed: 29336991]
37. Skinner SO, Sepulveda LA, Xu H & Golding I Measuring mRNA copy number in individual Escherichia coli cells using single-molecule fluorescent in situ hybridization. Nat Protoc 8, 1100–1113 (2013). [PubMed: 23680982]
38. Kong XN, et al. LPS-induced down-regulation of signal regulatory protein {alpha} contributes to innate immune activation in macrophages. J Exp Med 204, 2719–2731 (2007). [PubMed: 17954568]
39. Danino T, et al. Programmable probiotics for detection of cancer in urine. Sci Transl Med 7, 289ra284 (2015).
40. Armstrong AC, et al. Immunization with a recombinant adenovirus encoding a lymphoma idiotype: induction of tumor-protective immunity and identification of an idiotype-specific T cell epitope. J Immunol 168, 3983–3991 (2002). [PubMed: 11937555]
41. Haldimann A & Wanner BL Conditional-replication, integration, excision, and retrieval plasmid-host systems for gene structure-function studies of bacteria. J Bacteriol 183, 6384–6393 (2001). [PubMed: 11591683]
42. Gerdes K, et al. Mechanism of postsegregational killing by the hok gene product of the parB system of plasmid R1 and its homology with the relF gene product of the E. coli relB operon. EMBO J 5, 2023–2029 (1986). [PubMed: 3019679]
43. Derman AI, et al. Alp7R regulates expression of the actin-like protein Alp7A in Bacillus subtilis. J Bacteriol 194, 2715–2724 (2012). [PubMed: 22427628]

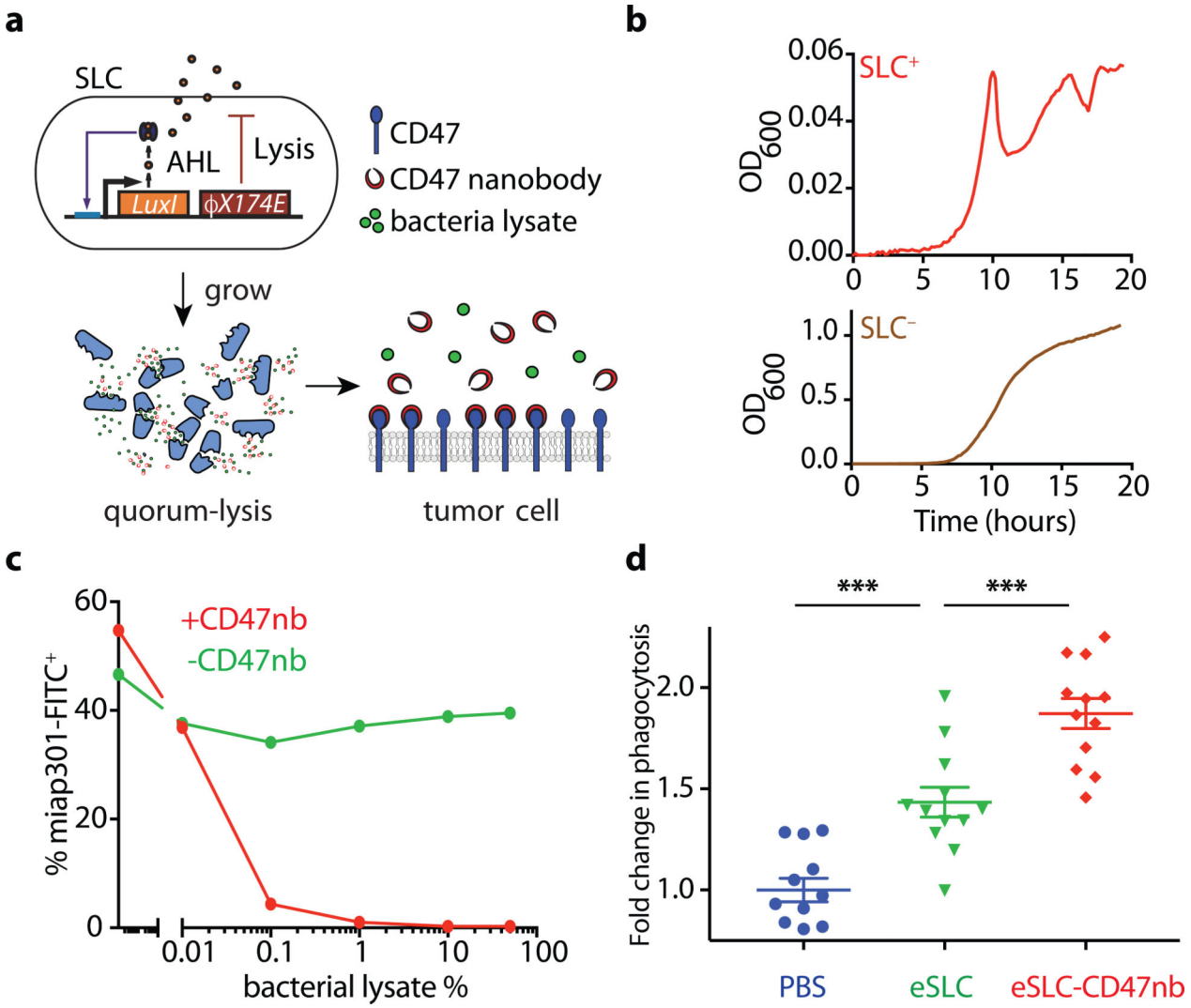

Figure 1 |. Quorum-induced release of functional anti-CD47 blocking nanobody by engineered immunotherapeutic bacteria encoding a synchronized lysis circuit (SLC).

a, *E. coli* with SLC reach a quorum and induce the phage lysis protein ϕX174E, leading to bacterial lysis and release of a constitutively produced, anti-CD47 blocking nanobody which binds to CD47 on the tumor cell surface. **b**, Bacterial growth dynamics over time of SLC^+ and SLC^- *E. coli* in batch liquid culture. Data are representative of three independent experimental replicates **c**, A20 cells were co-incubated with constant concentration of FITC conjugated αCD47 monoclonal antibody (FITC-miap301) along with varying concentrations of bacterial lysates containing constitutively expressed CD47nb (pSC02) or empty vector (pSC03). Data are representative of two independent experimental replicates **d**, *in vitro* phagocytosis of DiI labeled A20 cells pretreated with PBS, SLC^+ bacteria lysate or SLC^+ $CD47nb^+$ bacteria lysate by bone-marrow derived macrophages (n= 4 fields of view × 3 replicates, *** P<0.001, one-way ANOVA with Bonferroni's multiple comparisons test)

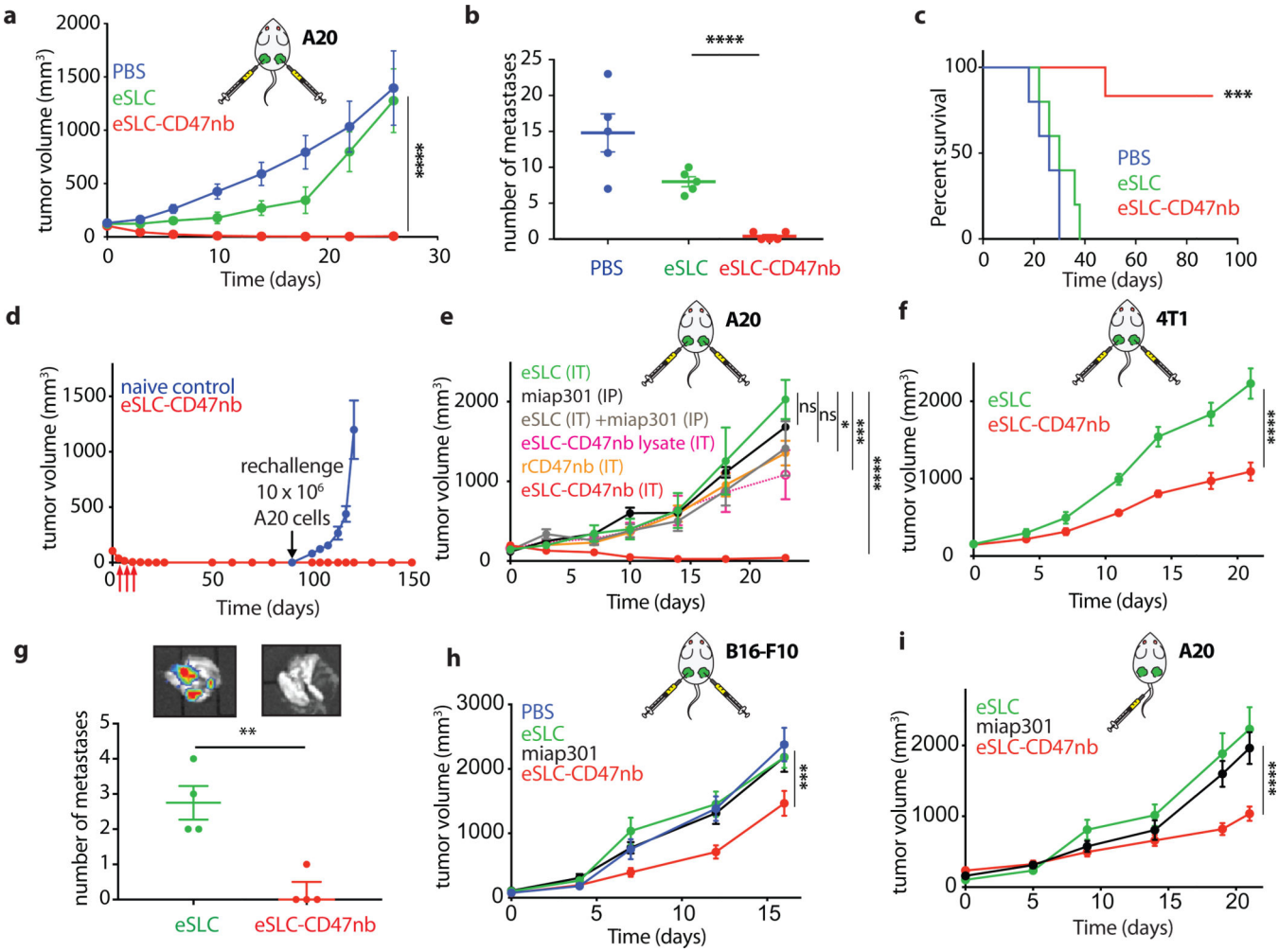

Figure 2 |. Intratumoral production of CD47 nanobody by eSLC elicits antitumor responses in multiple syngeneic murine tumor models

a, BALB/c mice (n=7 per group) were implanted subcutaneously with 5×10^6 A20 B-cell lymphoma cells on both hind flanks. When tumor volumes were 100–150 mm^3, mice received intratumoral injections every 3–4 days with PBS, eSLC or eSLC-CD47nb in both tumors. Tumor growth curves (**** P<0.0001, two-way ANOVA with Tukey's multiple comparisons test, error bars represent s.e.m.). Data are representative of two independent experimental replicates **b**, Quantification of metastatic nodules present in livers on day 30 following bacterial therapy (n= 5 per group, **** P<0.0001, unpaired t-test). **c**, Kaplan-Meier survival curves for A20 tumor bearing mice (n=5 per group, ***P<0.001, Log-rank (Mantel-Cox test)). **d**, Mice that had completely cleared A20 tumors were re-challenged with 10×10^6 A20 cells on day 90 following initial treatment. Naive mice received 5×10^6 A20 cells in each flank (n=4 mice per group). **e,** When A20 tumor volume reached 100–150 mm^3 mice received intratumoral injections of eSLC, eSLC-CD47nb bacterial lysate, recombinant CD47nb (rCD47nb, 50 μg) and eSLC-CD47nb, or intraperitoneal injections of anti-CD47 mAb (clone miap-301, 400 μg) alone or in combination with intratumoral eSLC for a total of 4 doses every 3–4 days. Tumor growth curves (n=4–8 per group, **** P<0.0001, *** P<0.001, two-way ANOVA with Tukey's multiple comparisons test, error

bars represent s.e.m.). **f**, Tumor growth curves. BALB/c mice (n=6–8 per group) were implanted subcutaneously with 10^6 4T1-Luciferase mammary carcinoma cells. When tumors reached a volume of 200 mm^3 mice were randomized and received intratumoral injections of PBS, eSLC, or eSLC-CD47nb every 3 days for a total of 4 doses (**** P<0.0001, two-way ANOVA with Tukey's multiple comparisons test, error bars represent s.e.m.). Data are representative of two independent experimental replicates. **g**, IVIS images of lungs extracted from 4T1-Luciferase hind-flank tumors and quantification of number of 4T1-Luciferase metastatic foci in lungs of mice treated with PBS, eSLC or eSLC-CD47nb (** P<0.01, unpaired t-test). **h,** Tumor growth curves from C57BL/6 mice subcutaneously injected with 5×10^5 B16-F10 melanoma cells into the hind flank. When tumors reached a volume of ~50–150 mm^3 mice were randomized and received intraperitoneal injections of miap301 (400 μg) or intratumoral injections of PBS, eSLC, or eSLC-CD47nb every 3 days for a total of 4 doses. (n=8–12 per group. *** P<0.001, two-way ANOVA with Tukey's multiple comparisons test, error bars represent s.e.m.). **i**, BALB/c mice were injected with 5×10^6 A20 cells into both hind flanks. When tumor volume reached 100–200 mm^3 mice received intravenous injections of eSLC or eSLC-CD47nb or intraperitoneal injections of miap301 CD47mAb (400μg), (n=8–10 per group, **** P<0.0001 twoway ANOVA with Tukey's multiple comparisons test).

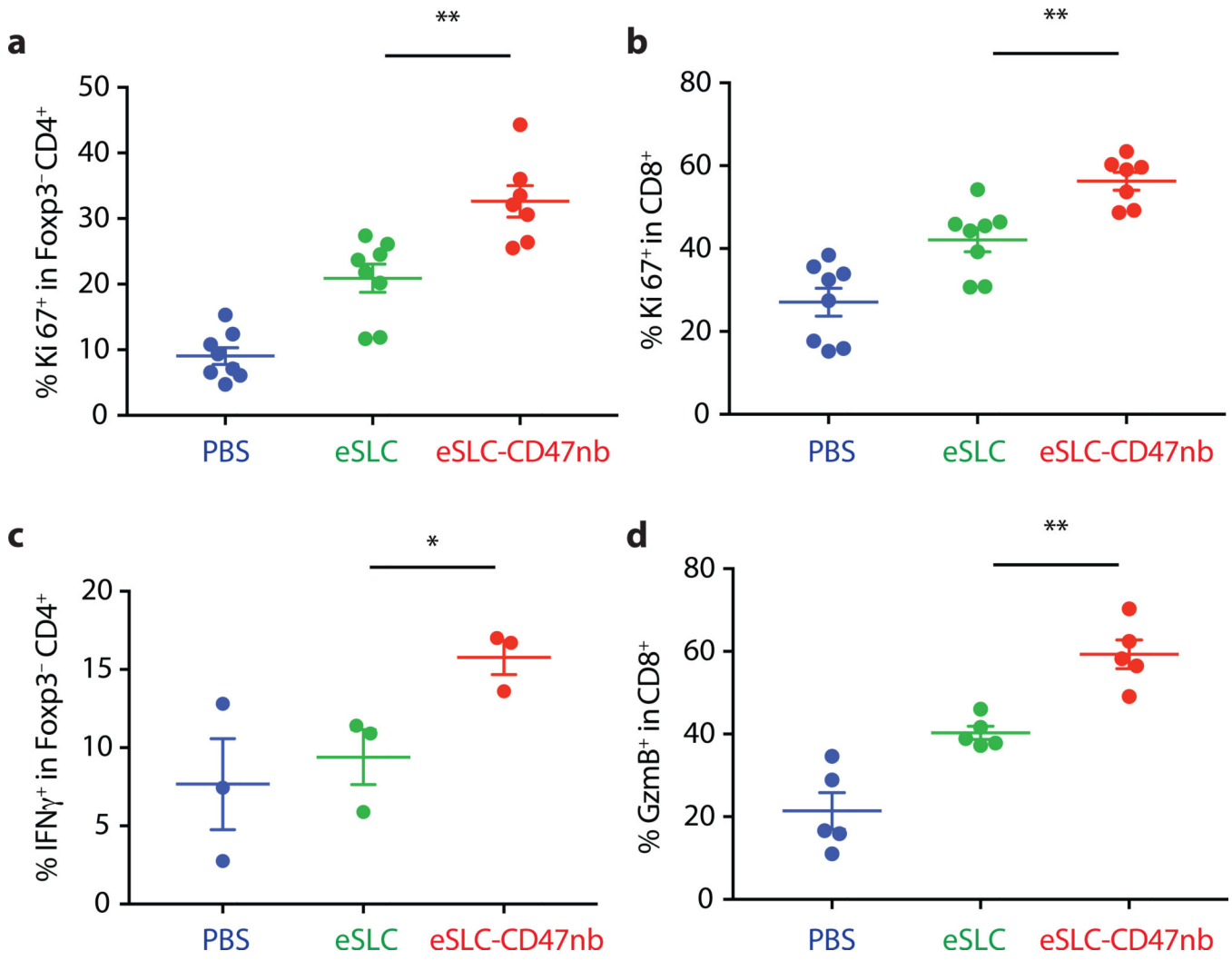

Figure 3 |. Immunotherapeutic eSLC-CD47nb bacteria prime robust adaptive antitumor immune responses.

5×10^6 A20 cells were implanted into the hind flanks of BALB/c mice. When tumors reached 100–150 mm^3 in volume (day 0), mice were treated with either PBS, eSLC or eSLC-CD47nb on days 0, 4 and 7. On day 8 tumors were homogenized and tumor-infiltrating lymphocytes were isolated for flow cytometric analysis on day 8. **a, b** Frequencies of isolated intratumoral Ki-67$^+$ Foxp3$^-$CD4$^+$ and CD8$^+$ T cells. **c,** Tumor infiltrating lymphocytes were stimulated following *ex vivo* isolation with PMA and ionomycin in the presence of brefeldin A. Frequencies of intratumoral IFNγ^+ Foxp3$^-$CD4$^+$ T cells following stimulation. **d,** Percentages of intratumoral Granzyme-B positive CD8$^+$ T cells. (n= 3–7 per group. * P<0.05, ** P<0.01, unpaired t-test, error bars represent s.e.m.). Data are pooled from two independent experimental replicates.

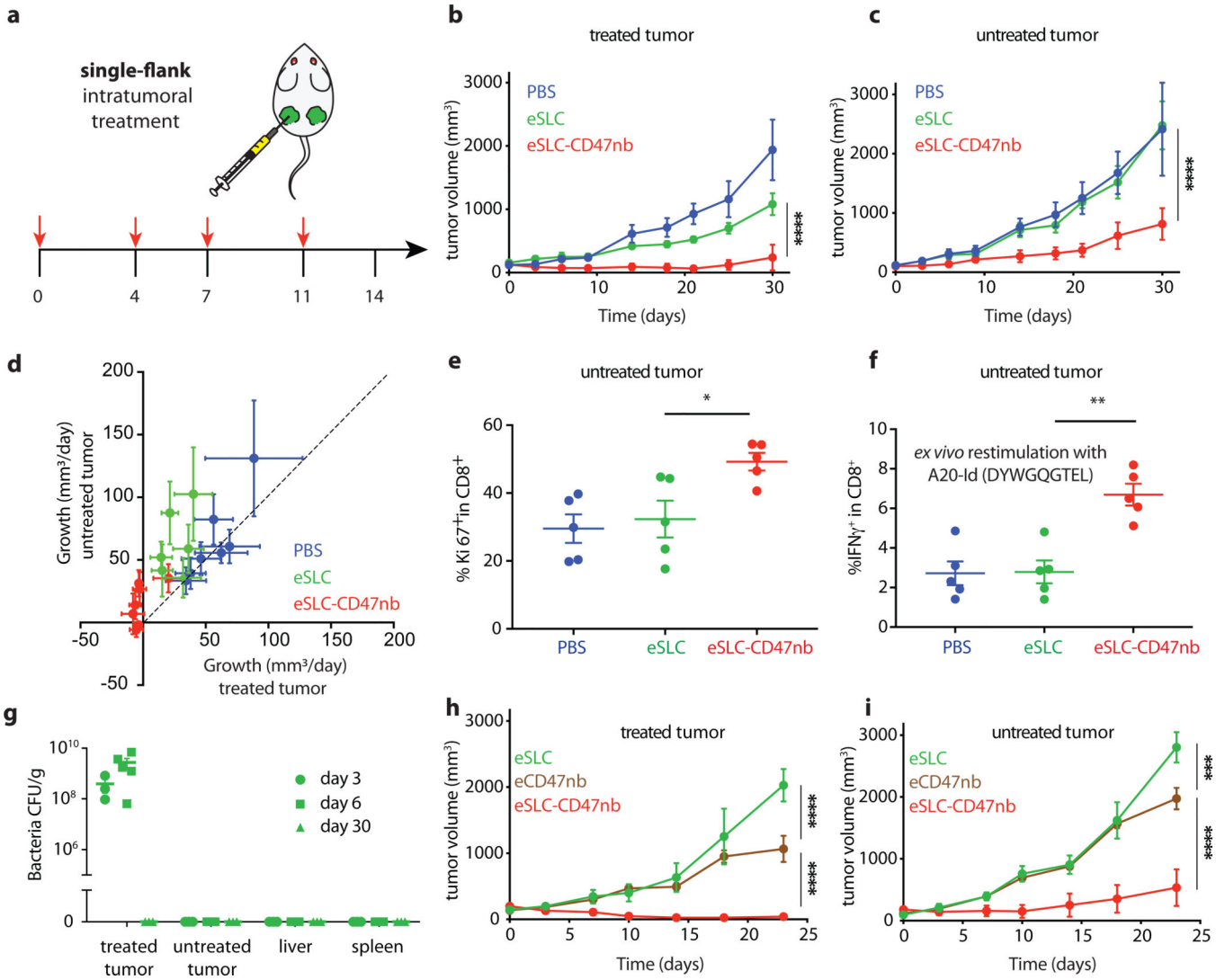

Figure 4 |. Systemic adaptive immunity following bacterial therapy limits growth of untreated tumors.

a, Treatment schedule. BALB/c mice (n=4 per group) were implanted subcutaneously with 5 × 10^6 A20 cells on both hind flanks. When tumor volumes reached 100–150 mm^3, mice received intratumoral injections every 3–4 days with PBS, eSLC or eSLC-CD47 into a single tumor. **b, c** Tumor growth curves of treated and untreated tumors (**** P<0.0001, two-way ANOVA with Tukey's multiple comparisons test, error bars represent s.e.m.). Data are representative of three independent experimental replicates **d**, Plot of untreated tumor growth rate (mm^3/day) vs. treated tumor growth rate (mm^3/day) for each mouse. Dotted line indicates slope=1, points represent means, error bars represent s.e.m. **e,** Untreated tumors were isolated on day 8 following single flank bacterial injections and analyzed by flow cytometry. Frequencies of intratumoral Ki-67^+ $CD8^+$ T cells (n=5 per group, * P<0.05, unpaired t-test, error bars represent s.e.m.). Data are representative of two independent experimental replicates. **f**, Tumor infiltrating lymphocytes were stimulated following *ex vivo* isolation with A20-Id peptide (DYWGQGTEL) in the presence of brefeldin A. Frequencies of intratumoral IFNγ^+ $CD8^+$ T cells (n=5 per group, ** P<0.01, unpaired t-test, error bars

represent s.e.m.) **g**, Biodistribution of SLC^+ *E. coli* on day 3, 6 and 30 following intratumoral bacterial injection. Excised tumors, livers and spleens were homogenized and plated on LB agar plates. Colonies were counted to determine CFU/g of tissue. Limit of detection 10^3 CFU/g (n=3–5 per time point). **h**, **i** Tumor growth curves of treated and untreated A20 tumors following unilateral intratumoral injections of eSLC, eCD47nb or eSLC-CD47nb every 3–4 days for a total of 4 doses (n=4 per group, *** P<0.001, **** P<0.0001, two-way ANOVA with Tukey's multiple comparisons test, error bars represent s.e.m.).